Apparent motion clustering on Cone-Beam fluoroscopic images for thorax tracking

Louise Grezes-Besset[1,2], Joël Schaerer[1,2], Patrick Clarysse[1], David Sarrut[1,2]

1: Université de Lyon, CREATIS-LRMN ; CNRS UMR 5220 ; Inserm U630 ; INSA-Lyon ; Université Lyon 1, F-69621, Villeurbanne, France.
2 : Centre de lutte contre le cancer Léon Bérard, F-69373, Lyon, France

Abstract

For lung cancer treatment with gated radiotherapy, tracking apparent respiratory motion in fluoroscopic images is an important step. The purpose of this study is to determine regions in the lung where the extracted apparent motion is homogeneous and reliable. Using an adapted block-matching algorithm on fluoroscopic sequences, we extracted individual point trajectories in region of interest corresponding to the lung and classified them using the k-means++ clustering algorithm. We then studied the apparent motion separately in each determined region. As a result, we obtained regions with homogeneous motion. Finally, we showed that regions in the lower part of the lung may be homogeneously correlated with an external signal acquired with an abdominal surrogate. This could be used in future work to estimate the parameters of a patient motion model obtained with the planning 4DCT.

Keywords

Fluoroscopic images, motion tracking, clustering, lung cancer

Introduction

For lung cancer treatment with gated radiotherapy, radiation is only delivered when the tumor is in a determined position. Various methods have thus been proposed to track the position of tumors using external signals or internal signals. External signals can be obtained with many devices such as a respiratory belt [1] or markers placed on the patient's abdomen [2]. External gating techniques rely on some correlation between these signals and the tumor location. External signals have the advantage of being non-invasive but their weakness is that the motion of external surrogates does not always accurately correspond with the tumor motion [3]. Internal motion is usually extracted from fluoroscopic images by different methods with implanted fiducial markers [4] or without them [5].

On fluoroscopic images, the real (3D) motion can only be evaluated according to the apparent (2D) motion. However, the apparent motion of internal structures can be different in phase and magnitude within the lung. For example, apparent motion is different if the tumor is located in the upper part of the lung or near the diaphragm. The analysis of apparent respiratory motion is therefore one important step to motion-adapted radiation therapy. We propose to study here how homogeneous is the apparent motion in the lung and which regions can or cannot be used to get a reliable gating signal.

Based on a block-matching motion extraction on cone-beam fluoroscopic sequences, we determine regions in the lung where the extracted motion is homogeneous and potentially more reliable. This extracted apparent motion could then be used to estimate the parameters of a patient motion prior model [6] obtained with the planning 4DCT.
To this end, we extract individual point trajectories and classify them using the k-means++ clustering algorithm [7]. We then study the apparent motion separately in each determined region. We finally study the correlation of the apparent motion in each of these regions with an external signal based on abdominal motion.

Material and methods

Data acquisition

Data was acquired on the Synergy system (Elekta) at the Léon Berard cancer center in Lyon, France. The system is composed of a kilo-voltage (kV) X-ray source mounted on the linac gantry, perpendicular to the mega-voltage source. It allows to reconstruct 3D cone-beam images from projections acquired from rotating views. Alternatively, a sequence of 2D+t fluoroscopic images from fixed viewpoint can be acquired. Two patients underwent a fluoroscopic session prior to conventional radiation treatment. The angle of projection between the vertical position and the kV source was 90° (viewing point in front of the patient face). The fluoroscopic sequence was made of 150 two-dimensional images

covering approximately 30s, i.e 7 respiratory cycles (Figure 1a).

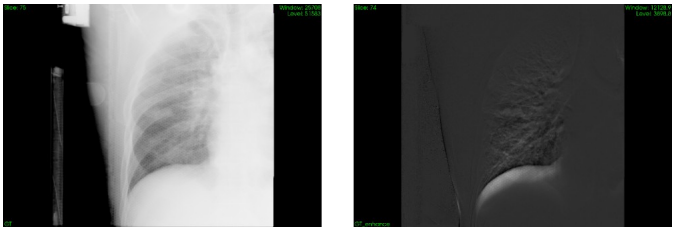

Figure 1: a- One image from fluoroscopic sequence. b- Same image after motion-enhanced filter.

During each session, an external signal was acquired with a video camera which captures the motion of a target located on the patient's abdomen. The synchronization between the external signal and the internal signal was obtained through a radiation sensor located in the treatment room and linked to a computer. When radiation was detected, the computer screen changed color. Thanks to a mirror, this color change was visible on the recorded video allowing to relate each frame of the video with corresponding kV acquisition.

Motion extraction

In order to remove static elements in the fluoroscopic sequence such as treatment table or patient's ribs, we applied a pre-processing filter which enhances motion (Figure 1b). Given a sequence of images, we computed the average image and subtracted this mean-image to each image of the sequence

We extracted individual point trajectories on each point of a region of interest (ROI) using a block matching algorithm [8]. The ROI was a hand-made segmentation. Table 1 summarizes the data set. The block-matching was computed with a size of research of 40x40pixels² and the size of block was 21x91 pixels² (each pixel were 0.8x0.8mm²). With such parameters, the maximum authorized motion was 16.8x72.8mm². We use the correlation coefficient as the similarity measure.

	Tumor position	Number of extracted trajectories
Patient 1	left lung middle	57400
Patient 2	left lung middle	45046

Table 1: Dataset characteristics

Clustering

In order to segment the extracted trajectories into coherent regions, we used the k-means++ clustering algorithm. This algorithm uses the well-known Lloyd algorithm repetitively with random initializations, using a well-chosen probability distribution to select the initial barycenters. The clustering solution with the lowest energy is then chosen as the final result. In practice, this process gives consistently better results than the Lloyd algorithm, and can be repeated until no better solution is obtained. In our experiments, we found that running it ten times gave consistently good results.

We applied the clustering algorithm on the trajectories seen as vectors with 300 components, of which 150 representing the position on the x axis over time, and the rest for the y axis. The metric used was the standard Euclidean norm. Before computing the clustering algorithm on the data set, we subtracted the first element to each trajectory in order to make trajectories independent of the original point position. The algorithm was computed with a given number k of regions. To set k, we tested growing values from 2 to 20 and kept the minimum value from which significant regions did not change any more. We consider that a region is significant when it contains more than 5% of total trajectories. In order to delete spurious trajectories, we computed the clustering algorithm twice. The result of the first computation of the algorithm gave one or two significant regions. We then recomputed the algorithm on the union of these regions.

Correlation

In order to study how homogeneous a region determined with the k-means++ algorithm is, we computed the correlation coefficient (cc) in the x-direction (Left-Right) and the y-direction (cranio-caudal) between each point of a region and the corresponding barycenter. We also used this similarity measure to compare the external signal and each point of each region.

Results and Discussion

Homogeneous Regions

The first line of figure 2 shows results for patient 1 whereas the second line shows results for patient 2. The first row (a- and d-) represents the image issued from the first computation of the clustering algorithm. The blue region corresponds to the points where trajectories are heterogeneous. We recompute the k-means++ algorithm on the red region. Significant found regions are shown on the second row (b- and e-). For each patient, the tumor was located in the red region. The other colors are set arbitrarily. For Patient 1, we found 3 significant regions for k=8. For Patient 2, we found 4 significant regions for k=8. The third row (c- and f-) of figure 2 represents the motion of each barycenter in each region for each patient. Same colors are used in rows 2 and 3 of figure 2 (e.g. for Patient 1, the motion of the mean trajectory in the red region of figure 2b is represented in red in figure 2c).

In table 2, we report the mean correlation coefficient in the cranio-caudal direction calculated on the region where the tumor is located, between the barycenter and trajectories in each point of the region. We found similar results on the other regions.

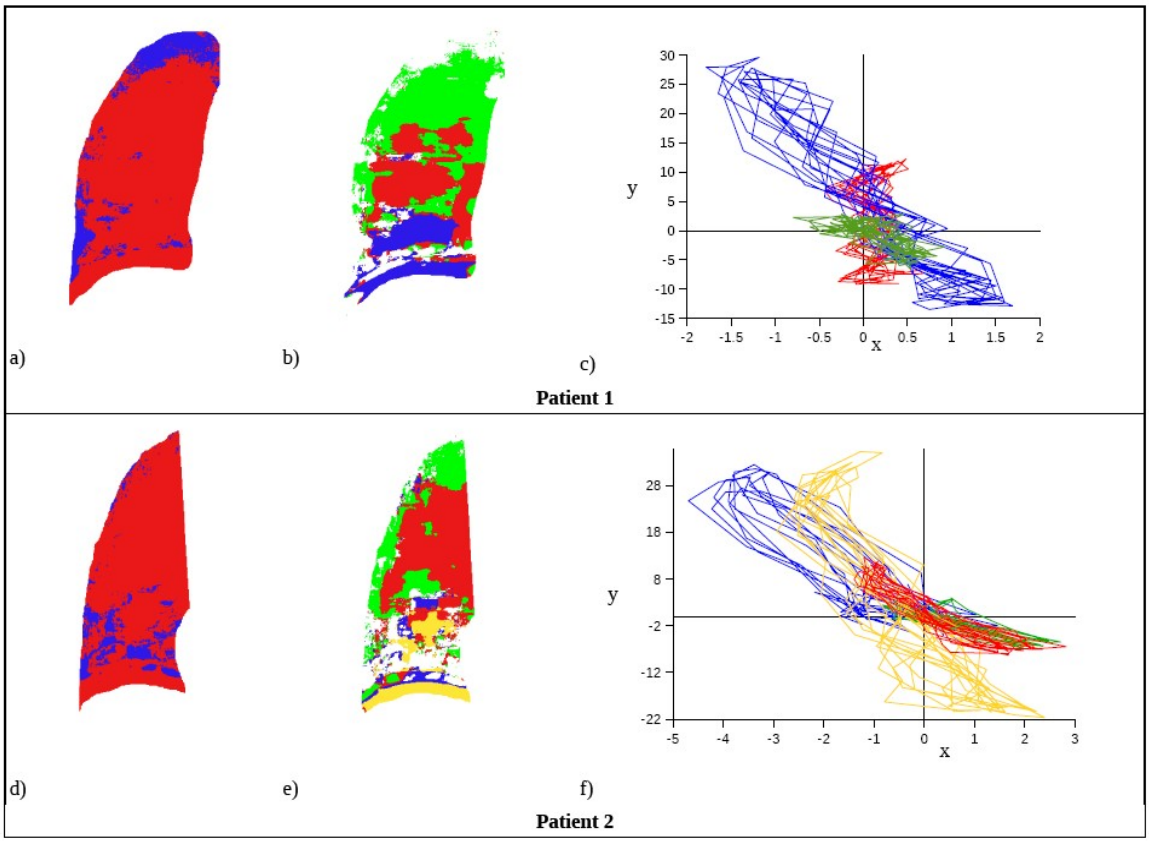

Figure 2: a- (respectively f-) red region represents non-spurious trajectories on patient 1 (resp. Patient 2). b- (respectively e-) labeled regions for patient 1 (resp. patient 2). c- (respectively f-) motion of the barycenter of each region for patient 1 (resp. patient 2).

	Patient 1	Patient 2
cc	0.90 (0.14)	0.88 (0.18)

Table 2: Mean correlation coefficient (standard deviation) between the barycenter and trajectories in each point of the region containing the tumor

As it is shown on figure 2, the k-means++ algorithm allowed to gather locations with similar trajectories into the same region with no geometrical a priori. This first result confirms that the extracted motion is locally coherent. The best homogeneity was always obtained in the cranio-caudal direction, where the motion is most significant.

Correlation with an external signal

In this section, we wanted to evaluate the correlation between the external signal and the apparent motion in each region. Considering labeled regions previously obtained on each patient, we compute the correlation coefficient between the external motion and the apparent trajectory of each point of each region. In table 3, we report the mean correlation coefficient and the standard deviation (sd) obtained in each region, for each patient. Colors refer to figure 2b (patient 1) and 2e (patient 2).

Figure 3 shows the motion in the cranio-caudal direction in the region containing the tumor and the external signal for Patient 1. To facilitate visualization, we rescale both trajectories between 0 and 1.

	label	cc (sd)
Patient 1	Green	-0.48 (0.28)
	Red (tumor)	-0.88 (0.14)
	Blue (diaphragm)	-0.91 (0.12)
Patient 2	Green	-0.38 (0.32)
	Red (tumor)	-0.84 (0.17)
	Yellow (diaphragm)	-0.93 (0.09)
	Blue	-0.64 (0.25)

Table 3:Mean correlation coefficient (standard deviation) between the external motion and trajectories in each point of the region containing the tumor

Figure 4 presents an image of the correlation coefficient between the external signal and the cranio-caudal motion of each point of the region containing the tumor for Patient 1. Similar results are obtained for Patient 2.

Results show that the correlation between the external signal and the apparent motion is good in the lower part of the lung, and even better in the region near the diaphragm (table 3). For each region, both signals are in phase opposition (cc<0 in table 3, see figure 3). If we focus on the region containing the tumor (in red), results show that the external signal and the apparent motion are well correlated on the major part of the region, except on the edges of the region, where the correlation coefficient decreases (see figure 4).

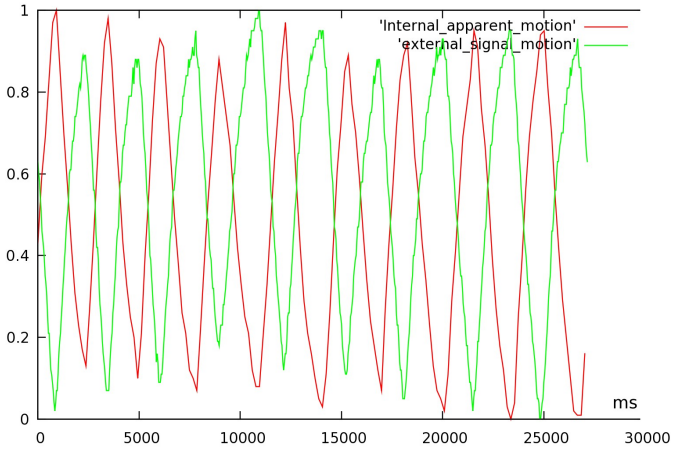

Figure 3: Cranio-caudal trajectories of the external signal (green) and the internal apparent motion (red) in the region containing the tumor.

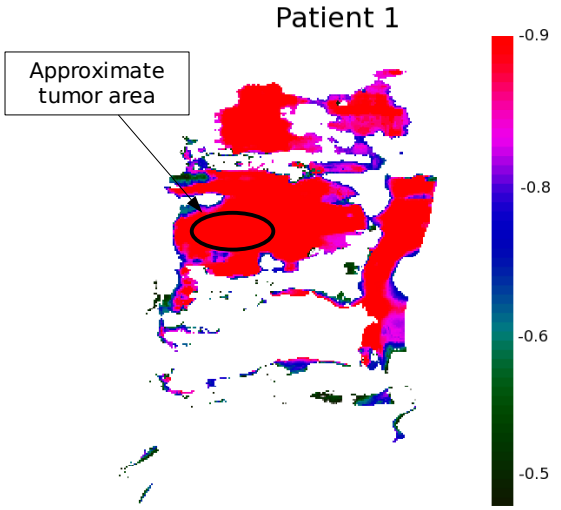

Figure 4: Image of correlation coefficient between the external signal and each trajectory of the region containing the tumor

This study enabled us to detemine homogenous regions in the lung where internal apparent motion and external motion are well correlated. We expect this method to be useful for the determination of a correlation function between external and internal signals, computed during a learning phase, prior to treatment. During the treatment phase, the apparent motion could then be tracked with the external signal and regularly checked with fluoroscopic acquisitions.

Conclusion

The analysis of apparent respiratory motion is an important step to lung cancer treatment with gated radiotherapy. In this study, we extracted the internal apparent motion with an adapted block-matching algorithm on fluoroscopic sequences. Based on the k-means++ clustering algorithm, we defined regions in which apparent motion is homogeneous. Finally, we showed that the region in the lower part of the lung is homogeneously correlated with an external signal acquired with an abdominal marker

In future works, we will work on determining a prediction function allowing to derive the motion model parameters from the apparent trajectories. As trajectories inside a given region are homogeneous, we expect this prediction function to be fairly robust.

References

[1] Allen Li X, Stepaniak C and Gore E 2006. Technical and dosimetric aspects of respiratory gating using a pressure-sensor motion monitoring system. *Med Phys* **33** 145-154

[2] Vedam SS, Keal P J, Kini V R, Mostafavi H, Shukla H P and Mohan R. 2003 Determining parameters for respiration-gated radiotherapy. *Med Phys* **28** 2139-2146

[3] Gierga D P, Brewer J, Sharp G C, Betke M, Willett C G and Chen G T Y. 2005 The correlation between internal and external markers for abdominal tumors : implications for respiratory gating. *Int J Radial Oncol Biol Phys* **61** 1551-1558

[4] Shirato H, Harada T, Harabayashi T, Hida K, Endo H, Kitamura K, Onimaru R, Yamazaki K, Kurauchi N, Shimizu T, Shinohara N, Matsushita M, Dosaka-Akita H and Miyasaka K. 2003 Feasibility of insertion/implantation of 2.0-mm-diameter gold internal fiducial markers for precise setup and real-time tumor tracking in radiotherapy. *Int J Radiat Oncol Biol Phys* **56** 240-247

[5] Berbeco R I, Mostafavi H, Sharp G C, Jiang S B. 2005 Towards fluoroscopic respiratory gating for lung tumours without radiopaque markers. *Phys Med Biol* **50** 4481-4490

[6] Vandemeulebroucke J, Kybic J, Clarysse P and Sarrut D. 2009 Respiratory Motion Estimation from Cone-Beam Projections Using a Prior Model. *Proc Medical Image Computing and Computer-Assisted Intervention* ed Yang G Z, Hawkes D, Rueckert D, Noble A and Taylor C pp 365-372

[7] Rit S, Sarrut D and Ginestet C 2005 Respiratory signal extraction for 4D CT imaging of the thorax from cone-beam CT projections. *Medical Image Computing and Computer-Assisted Intervention*, ed J. Duncan and G. Gerig, pp 556-63.

[8] Arthur D and Vassilvitskii S. 2007 k-means++: the advantages of careful. *Proc 18th ACM-SIAM symposium on Discrete algorithms* 1025-1035.